Title

Ni Foam-Supported Fe-Doped β-Ni(OH) 2 Nanosheets Show Ultralow Overpotential for Oxygen Evolution Reaction

Journal

ACS Energy Letters, 4(3)

ISSN

2380-8195

Authors

Kou, T
Wang, S
Hauser, JL
et al.

Publication Date

2019-03-08

DOI

10.1021/acsenergylett.9b00047

Peer reviewed

Ni Foam Supported Fe-doped β-$Ni(OH)_2$ Nanosheets Shows Ultralow Overpotential for Oxygen Evolution Reaction

Tianyi Kou[†,§], *Shanwen Wang*[†,§], *Jesse L. Hauser*[†], *Mingpeng Chen*[†], *Scott R. J. Oliver*[†], *Yifan Ye*[‡], *Jinghua Guo*[‡], *and Yat Li*[†,*]

[†]Department of Chemistry and Biochemistry, [‡]Department of Physics, University of California, 1156 High Street, Santa Cruz, California, 95064, USA

[‡]Advanced Light Source, Lawrence Berkeley National Laboratory, Berkeley, CA 94720, USA

[§] These authors contributed equally to the work.

* Corresponding author: Yat Li (yatli@ucsc.edu)

Keywords

Oxygen evolution reaction, Fe doping, $Ni(OH)_2$ nanosheets, Alkaline media, ultralow overpotential, high intrinsic activity

Abstract

Oxygen evolution reaction (OER) involves multiple electron transfer processes, resulting in high activation barrier. Developing catalysts with low overpotential and high intrinsic activity towards OER is critical but challenging. Here we demonstrate a facile hydrothermal method of functionalizing Ni foam with Fe-doped β-$Ni(OH)_2$ nanosheets, which exhibit an overpotential of 219 mV at the geometric current density of 10 mA cm^{-2}. To our knowledge, it is the best value reported for Ni-/Fe hydroxide based OER catalyst. In addition, the catalyst achieves a current density of 6.25 mA cm^{-2} at the overpotential of 300 mV when it is normalized to the electrochemical surface area of catalyst. This value is better than most of the state-of-the-art OER catalysts. The enhanced catalytic activity is believed to be due to the unique combination of structural and chemical properties of the catalyst.

Electrolysis of water is one of most efficient and environmentally friendly methods to generate hydrogen gas, a chemical fuel with ultrahigh gravimetric energy density. High-efficiency, low-cost and stable catalysts are required for both cathode and anode to reduce the activation energy barriers for hydrogen and oxygen evolution reactions. Significant advances have been made lately in developing high-efficiency hydrogen evolution reaction (HER) catalysts, which are routinely reported to have overpotentials around or below 150 mV at j_{geo} (current density normalized to the geometric area of the electrode) of 10 mA/cm^2.[1] In comparison to HER that involves only two-electron transfer processes, oxygen evolution reaction (OER) taking place on the anode is a four-electron transfer process in which the multi-step elementary reactions create significant energy barriers.[2] As a result, most catalysts typically have high overpotentials close to or larger than 300 mV at j_{geo}=10 mA/cm^2 ,[2a] which poses a major limitation to the overall efficiency of water electrolysis. Further reduction of OER overpotential is therefore the key to high efficiency water splitting. Constructing an efficacious OER interface through catalysts design is critical in largely boosting the reaction kinetics. Classical IrO_x and RuO_2 are the benchmark OER catalysts with decent performances with overpotential typically close to 350 mV at 10 mA/cm^2.[3] Yet, their scarcity and inferior stability at higher anodic potentials

are the primary concerns.[4] Here we seek to develop an inexpensive, potent and robust OER catalysts.

First-row transition metals such as Ni and Fe are earth abundant and low cost materials. More importantly, they tends to have suitable chemical bond strength with catalytic reaction intermediates due to their unique 3d electronic structures, and thus, appealing for heterogeneous catalytic reactions including OER.[5] Previous studies have shown that the bond strength of metal-OH is one of the key factors determine OER activity in alkaline media .[6] Either too strong or too weak bond strength results in inferior performance according to the volcano plot. Ni and Fe are located at the opposite sides of the volcano plot, and therefore the combination of Ni and Fe are anticipated to be beneficial for achieving a balanced metal-OH bond strength.[6] Enormous efforts have been devoted to develop various types of NiFe OER catalysts. For example, NiFe-layered double hydroxide with abundant oxygen vacancies was found to be effective in reducing the adsorption energy barrier of OH, and achieved a low overpotential of 250 mV at j_{geo} of 10 mA/cm^2.[7] Fe doped crystalline β-Ni(OH)$_2$ nanoparticles were able to achieve a similar overpotential at 260 mV at j_{geo} of 10 mA/cm^2, suggesting the critical role of Fe in mediating the OER activity of Ni hydroxide.[8] Albeit the enormous progress in making better OER catalysts, it is always desirable while challenging to further decrease the OER overpotential and increase the total electrode activity of inexpensive NiFe catalysts. Total electrode activity is determined by both the catalyst's intrinsic activity and electrochemical

surface area (ECSA). Total electrode activity (geometric current density, j_{geo}) should be enhanced via improving the intrinsic activities (current density per unit of electrochemical surface area, j_{ECSA}) of catalyst, rather than increasing the mass loading of catalyst.[3b, 9]

Here we present a facile hydrothermal method of functionalizing Ni foam with Fe doped β-$Ni(OH)_2$ nanosheets for OER. These nanosheets achieve an outstanding overpotential of 219 mV at j_{geo} of 10 mA/cm^2, which is the best value reported for Ni hydroxide based OER catalysts at the same current density. Moreover, the j_{ECSA} of 6.25 mA/cm^2 at 300 mV obtained from the catalyst is also among the best reported values. Taken together, these results show that the incorporation of Fe is effective in improving the overpotential and the intrinsic activity of Ni based catalysts.

The synthesis of Fe doped β-$Ni(OH)_2$ nanosheets is illustrated in **Figure 1a**. Ni foam serves both as the substrate as well as the Ni source for the growth of $Ni(OH)_2$ nanosheets. The excellent electrical conductivity of Ni makes it a good current collector.[10] Its high porosity is also favorable diffusion of electrolytes and gas evolution during OER process. Ni foam hydrothermally treated in iron (III) nitrate nonahydrate for 5 hours at 150 °C results in an uniform coverage of vertically aligned nanosheets (**Figure 1b**), which are characterized to be β-$Ni(OH)_2$ (**Figure S1**). The as-synthesized nanosheets were further treated by cyclic voltammetry conditioning (experimental section) in 1.0 M KOH to improve the wetting of electrode surface. The phase and chemical composition of β-$Ni(OH)_2$ were remained

unchanged after CV conditioning (**Figure S1**), while the flat nanosheets were turned into crumpled structures (**Figure 1c-d**). This morphological change is believed to be due to the intercalation/deintercalation of ions (such as K^+ in the electrolyte) into the layered β-$Ni(OH)_2$ structures during CV conditioning. Transmission electron microscopy (TEM) images revealed that the β-$Ni(OH)_2$ nanosheet is a mixture of crystallized and amorphous structure (**Figure 1e-g**). The interpenetrated crystallized and amorphous structures create kink sites enriched boundaries on which the under-coordinated atoms are generally known for facilitating adsorptions.[11] The inter-spacings of the observed lattice fringes are consistent with the *d*-spacing of (002) and (101) crystal planes of β-$Ni(OH)_2$. Elemental mapping data confirmed the uniform distribution of Ni, Fe and O in the entire nanosheet (**Figure 1h**), indicating the successful incorporation of Fe into the β-$Ni(OH)_2$ structures. The Fe concentration can be controlled by adjusting the amount of Fe precursor, as shown in **Table S1** (Supporting Information). Four Fe-doped β-$Ni(OH)_2$ samples were prepared under the same hydrothermal conditions using different amount of iron (III) nitrate nonahydrate (0 mg, 1.8 mg, 3.6 mg and 7.2 mg), they are denoted as Ni-Fe-0, Ni-Fe-1, Ni-Fe-2 and Ni-Fe-3, respectively. Notably, adjusting the amount of Fe precursor change neither the morphology nor crystal phase of β-$Ni(OH)_2$ (**Figure S2, Supporting Information**).

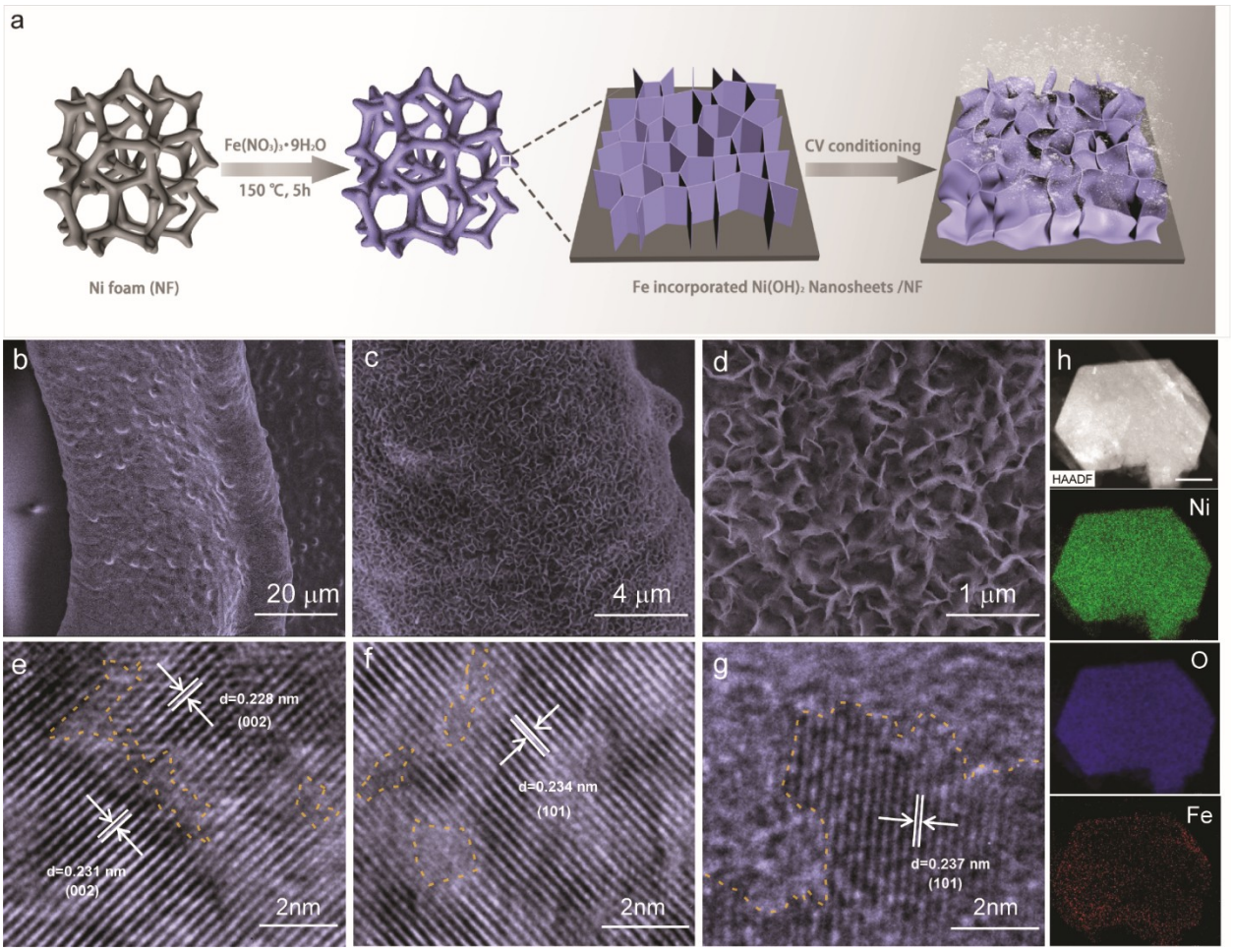

Figure 1. (a) Schematic illustration of the synthesis of Fe-doped $Ni(OH)_2$ nanosheets/NF. (b-d) Scanning electron microscopy (SEM) images of the Fe-$Ni(OH)_2$ nanosheets/NF. (e-g) High resolution TEM images obtained from a Fe-$Ni(OH)_2$ nanosheet. Dashed lines highlight the edge of the interrupted lattice. (h) High angle annular dark field-TEM image of a Fe-$Ni(OH)_2$ nanosheet and the corresponding elemental mapping image of Ni, Fe, and O. Scale bar is 100 nm.

To probe the local structure and valence state of the Fe-doped β-$Ni(OH)_2$ samples, Ni and Fe K-edge X-ray absorption spectroscopy (XAS) data (**Figure**

2) were recorded at beamline 10.3.2 of the Advanced Light Source, Berkeley, Lawrence Berkeley National Laboratory, CA [Marcus 2004]. The white line of the Ni K-edge spectrum of Ni-Fe-2 is centered at 8350 eV (**Figure 2**), corresponding to Ni^{2+} as previously reported in the literature[12]. Ni K-edge EXAFS data evidenced an extra peak at 1.2 *Å*, corresponding to a Ni-O bond, when compared with the Ni foil spectrum showing only Ni-Ni coordination. Overall Ni XAS data showed clear evidence of the successful growth of $Ni(OH)_2$ on the Ni substrate. Further, Fe K-edge XANES data on the Fe dopant in the Ni-Fe-2 sample show a white line peak at 7130.4 eV associated with the 1s to 4p dipole transition, suggesting the presence of oxidized Fe (**Figure 2b**)[13] .The Fe XANES data could not be fitted nor the oxidation state determined due to poor signal quality. Overall, XAS results confirmed the substitutional doping of oxidized Fe in β-$Ni(OH)_2$ structures and Fe remains in oxidized form.

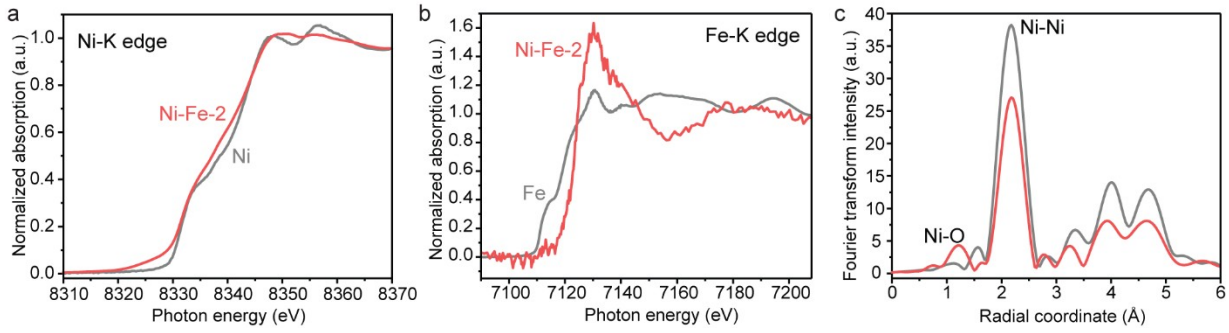

Figure 2. (a) Ni K-edge XANES spectra of Ni-Fe-2 and Ni foil. (b) Fe K-edge XANES spectra of Ni-Fe-2 and Fe foil. (c) Magnitude of the Fourier-transformed Ni K-edge EXAFS spectra.

The catalytic performances of the Fe doped β-$Ni(OH)_2$ nanosheets for OER were investigated through linear sweep voltammetry (**Figure 3a**) conducted in O_2 saturated 1.0 M KOH electrolyte. The anodic oxidation peaks in the polarization curves correspond to the conversion of β-$Ni(OH)_2$ to β-NiOOH, which is believed to be the active catalyst for OER.[14] Dramatically increased current after the oxidation peak indicates the rigorous OER process. Overpotentials at the geometric current density of 10 mA/cm^2 were measured for the evaluation of total electrode activity.[15] As shown in Figure 3a, the bare Ni foam has the largest overpotential of 305 mV at j_{geo}=10 mA/cm^2. The growth of $Ni(OH)_2$ nanosheets on Ni foam (Ni-Fe-0) significantly reduces the overpotential and boosts the total electrode activity, as $Ni(OH)_2$ is believed to be more favorable for the adsorption of OER intermediate such as OH than Ni foam. All Fe doped β-$Ni(OH)_2$ samples show even lower overpotential than Ni-Fe-0. Among them, Ni-Fe-2 exhibits the lowest overpotential of 219 mV at j_{geo}=10 mA/cm^2, which is the best value reported for Ni-/Fe hydroxide based OER catalysts (**Table 1**), obtained at the same geometric current density in the same electrolyte (1.0 M KOH). An average overpotential of 219.6 mV at 10 mA/cm^2 was obtained from four different Ni-Fe-2 samples (**Figure S3**), confirming the results are highly reproducible. All

the three Fe doped β-$Ni(OH)_2$ samples have similar Tafel slopes between 53 mV/dec and 57 mV/dec, which are slightly smaller than the values obtained from β-$Ni(OH)_2$ (61 mV/dec) and bare Ni foam (64 mV/dec), as shown in **Figure 3b**. Tafel slope has been used to analyze the kinetics of OER rate-determining step.[16] The Tafel slopes of 53-57 mV/dec suggests that •OH adsorption is favorable on the surface of Fe doped β-$Ni(OH)_2$ nanosheets, while the subsequent step with deprotonation of ¿OH (¿ is the active site) is the rate-determining step.

The total electrode activity is determined by the total number of active sites and the intrinsic activity of each individual active site. The number of active sites is typically proportional to the electrochemical surface area (ECSA). **Figure 3c** shows the plots of the difference of anodic and cathodic current density versus the scan rate, in which the slope of the curves (areal capacitance) is proportional to their ECSA. Ni-Fe-2 has the highest areal capacitance of 2.96 mF/cm^2, which are substantially higher than the other samples. The results suggest that Ni-Fe-2 has the highest number of active sites, which is expected to be determined by its compositional and structural features such as Fe doped amorphous/crystalline interface. Furthermore, the higher number of active sites is favorable for charge transfer. Electrochemical impedance spectroscopy (EIS) studies were conducted for Fe-doped β-$Ni(OH)_2$ samples and the control samples (**Figure 3d**). The EIS results are fitted based on the equivalent circuit (**Figure 3d inset**) and the obtained solution resistance (R_s) and charge transfer resistance (R_{ct}) are

summarized in **Table S2** (Supporting Information). As expected, Ni-Fe-2 has the smallest R_{ct} of 2.971 Ω/cm^2, which is considerably smaller than the values obtained from Ni-Fe-0 (7.120 Ω/cm^2), Ni-Fe-1 (7.077 Ω/cm^2) and Ni-Fe-3 (8.120 Ω/cm^2), respectively. The Ni foam has the highest R_{ct} of 30.45 Ω/cm^2 due to the lack of OER active sites. It is also noteworthy that all Fe-doped β-$Ni(OH)_2$ samples have fairly small values of R_s that is comparable to the value of bare Ni foam, ensuring efficient charge transport.

To determine the intrinsic activity of individual active site, we normalize the OER current to ECSA (j_{ECSA}). As shown in **Figure 3e**, Ni-Fe-2 achieves j_{ECSA} of 10 mA cm^{-2} at fairly low overpotential of 316 mV. At the same overpotential, Ni-Fe-0, Ni-Fe-1 and Ni-Fe-3 exhibit significantly lower j_{ECSA} of 3.7, 7.0 and 4.5 mA cm^{-2}, respectively and the bare Ni foam has the worst j_{ECSA} of only 1.2 mA cm^{-2}. It is clear that the intrinsic activity of β-$Ni(OH)_2$ is significantly better than the Ni foam substrate, and the introduction of right amount of Fe doping can further boost its intrinsic activity towards OER. Most importantly, the results also confirmed that the excellent catalytic activity of Ni-Fe-2 is not only due to the increased ECSA but also the enhanced intrinsic activity of each active site in converting OH^- into oxygen gas. The intrinsic activity of Ni-Fe-2 is substantially better than many other state-of-the-art OER catalysts (**Figure 3f**). In addition, the Ni-Fe-2 was able to retain almost the same OER catalytic performance after testing for 10000 cycles (**Figure S4, Supporting Information**), showing its excellent stability.

To summarize, the outstanding catalytic activity of Ni-Fe-2 can be attributed to several factors. First, the vertically aligned crumpled nanosheets offer large number of highly accessible active sites. Second, the good porosity of the nanosheet network allows rapid release of oxygen gas bubbles during OER, which otherwise would pose a physical barrier between the active sites and electrolytes.[17] Third, we believe that the co-existence of amorphous and crystal microstructures on the Fe-doped β-$Ni(OH)_2$ nanosheets may also contribute to the improved catalytic activity. Although amorphous structures usually have lower electrical conductivity than crystalline materials because of its long-range disorder, the surface heterogeneity would expose additional active sites for OER.[18] The boundaries between crystalline and amorphous structures represents the under-coordination positions and generally serve as the preferential adsorption sites towards the reactants in OER.[19] Finally, recent theoretical simulations also found that the Fe dopants serve as active sites owing to its appropriate adsorption strength towards the OER intermediates, and its strong electron-withdrawing effect turns the surrounding of Ni to the ‘hot-spot’ for OER.[20] This work demonstrate an inexpensive catalyst with ultralow overpotential and outstanding intrinsic catalyst activity. The findings also provide important guidelines for design and synthesis of Ni based OER catalysts.

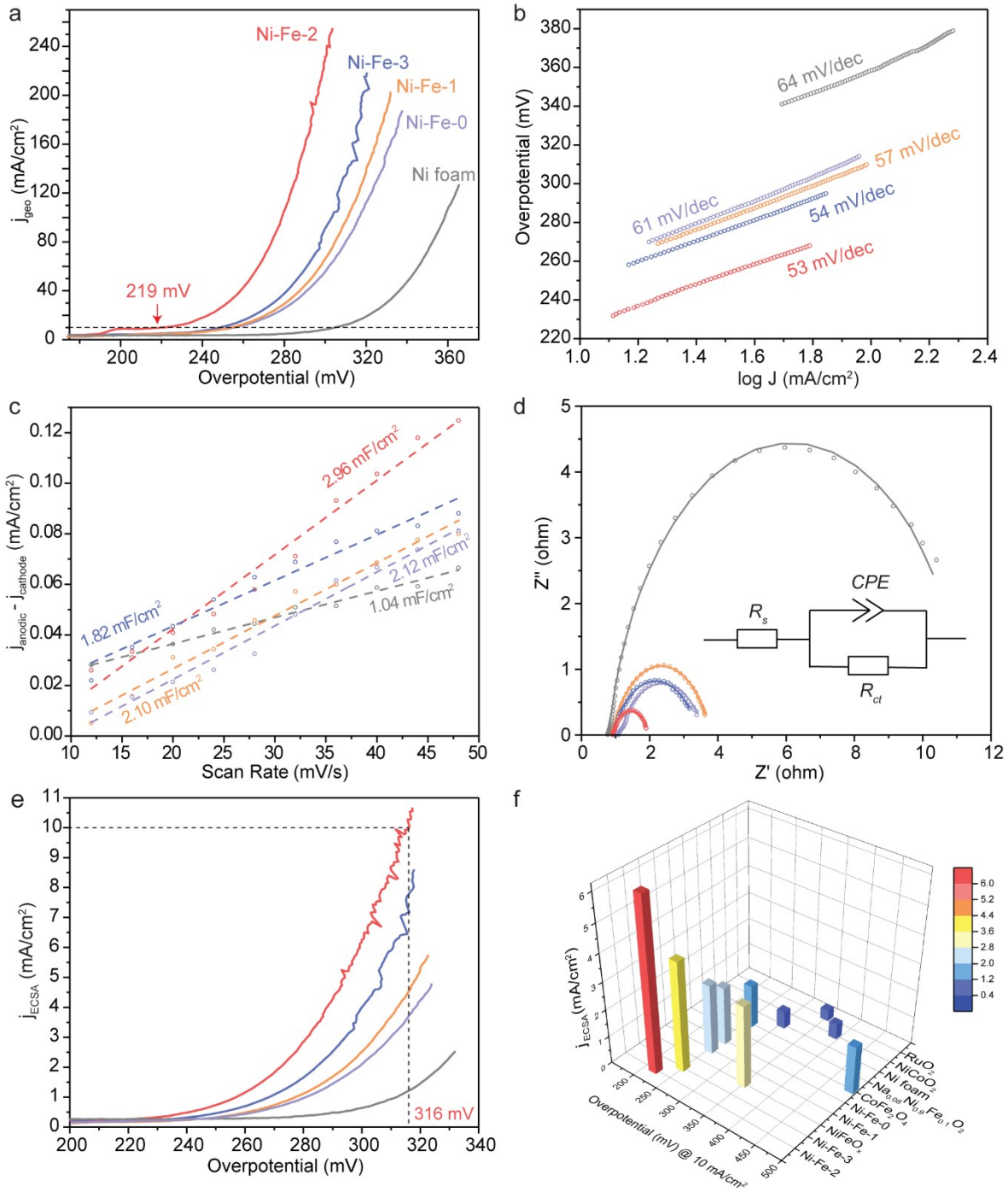

Figure 3. (a) OER polarization curves obtained from Ni-Fe-0, Ni-Fe-1, Ni-Fe-2, Ni-Fe-3 and Ni foam in 1.0 M KOH solution at a scan rate of 1 mV/s. Dashed line corresponding to 10 mA/cm^2. (b) Tafel plots of the samples. The values are the slope of each curves. (c) Plots of difference of anodic and

cathodic current density as a function of scan rate; (d) Electrochemical impedance spectra of the samples collected at the overpotential of 291 mV, with frequency from 100 kHz to 1 Hz and amplitude of 5 mV. Dots and lines represent the experimental and simulated data, respectively. (e) Polarization curves of the samples with current density normalized to ECSA. (f) 3D histogram compares the ECSA current densities and overpotentials at 10 mA/cm^2 of Fe-doped β-$Ni(OH)_2$ samples with other state-of-the-art OER catalysts including $NiCoO_2$,[3b] $NiFeO_x$,[21] $CoFe_2O_4$,[22] $Na_{0.08}Ni_{0.9}Fe_{0.1}O_2$,[23] RuO_2,[23].

Table 1. Comparisons of OER performance of Ni-/Fe (oxy)hydroxide based catalysts

Catalyst	Overpotential (mV) at j_{geo}=10 mA/cm^2	Scan rate (mV/s)	References
Fe-doped β-$Ni(OH)_2$ nanosheets/Ni foam	219	1	**This work**
Fe-doped β-$Ni(OH)_2$ nanoparticles	260	10	8
Fe-doped β-NiOOH films	340	10	24
NiFe-LDH nanoplates array	224	10	25
NiFe-LDH nanoplates films	250	1	26
NiFe-LDH nanosheets	300	5	27
Ni nanoparticles/NiFe LDH	320	5	28
NiFe-LDH/CNT	230	5	29
$Ni_{2/3}Fe_{1/3}$-LDH/rGO	240	5	30
NiFe-LDH/graphene and CNT	350	10	31
Ni(Fe)OOH films	260	_	32

Conclusions

In conclusion, in this work we present a facile hydrothermal method of functioning Ni foam with Fe doped β-$Ni(OH)_2$ nanosheets as efficient OER catalysts. The as-synthesized Fe incorporated β-$Ni(OH)_2$ nanosheets show an overpotential of 219 mV at the geometric current density of 10 mA cm^{-2}, and a low Tafel slope of 53 mV dec^{-1}, suggesting its competing total electrode activity. Quadruplicate measurements of the Ni-Fe catalysts with small standard deviation of 3.5 mV indicate the great reproducibility of this method. In addition to the total electrode activity, a large ECSA current density of 6.25 mA cm^{-2} at 300 mV confirms its high intrinsic activity. The achieved high total electrode and intrinsic activity of the Ni-Fe catalysts should be attributed to its beneficial structural and compositional merits including porous structures facilitating the diffusion of electrolytes as well as avoiding the accumulation of gas bubbles, long-range disorders in amorphous structure co-existing with the kink enriched crystalline structure offering enriched active sites for the OER process, and Fe dopant introducing additional active sites for appropriate OH adsorptions and thus enhanced OER activity.

Acknowledgements

This research used resources of the Advanced Light Source, which is a DOE Office of Science User Facility under contract no. DE-AC02-05CH11231.

References

1. (a) Tianyi, K.; Tyler, S.; Bin, Y.; Irwin, C.; David, T.; Yuan, P.; Yat, L., Theoretical and Experimental Insight into the Effect of Nitrogen Doping on Hydrogen Evolution Activity of Ni3S2 in Alkaline Medium. *Advanced Energy Materials* **2018,** *8* (19), 1703538; (b) Wu, Y.; Liu, Y.; Li, G.-D.; Zou, X.; Lian, X.; Wang, D.; Sun, L.; Asefa, T.; Zou, X., Efficient electrocatalysis of overall water splitting by ultrasmall NixCo3−xS4 coupled Ni3S2 nanosheet arrays. *Nano Energy* **2017,** *35*, 161-170; (c) Yu, M.; Zhao, S.; Feng, H.; Hu, L.; Zhang, X.; Zeng, Y.; Tong, Y.; Lu, X., Engineering Thin MoS2 Nanosheets on TiN Nanorods: Advanced Electrochemical Capacitor Electrode and Hydrogen Evolution Electrocatalyst. *ACS Energy Letters* **2017,** *2* (8), 1862-1868; (d) Zhang, J.; Wang, Y.; Zhang, C.; Gao, H.; Lv, L.; Han, L.; Zhang, Z., Self-Supported Porous NiSe2 Nanowrinkles as Efficient Bifunctional Electrocatalysts for Overall Water Splitting. *ACS Sustainable Chemistry & Engineering* **2018,** *6* (2), 2231-2239.
2. (a) Tahir, M.; Pan, L.; Idrees, F.; Zhang, X.; Wang, L.; Zou, J.-J.; Wang, Z. L., Electrocatalytic oxygen evolution reaction for energy conversion and storage: A comprehensive review. *Nano Energy* **2017,** *37*, 136-157; (b) Xu, Z.; Yipu, L.; Guo-Dong, L.; Yuanyuan, W.; Da-Peng, L.; Wang, L.; Hai-Wen, L.; Dejun, W.; Yu, Z.; Xiaoxin, Z., Ultrafast Formation of Amorphous Bimetallic Hydroxide Films on 3D Conductive Sulfide Nanoarrays for Large-Current-Density Oxygen Evolution Electrocatalysis. *Advanced Materials* **2017,** *29* (22), 1700404.
3. (a) Nong, H. N.; Oh, H.-S.; Reier, T.; Willinger, E.; Willinger, M.-G.; Petkov, V.; Teschner, D.; Strasser, P., Oxide-Supported IrNiOx Core–Shell Particles as Efficient, Cost-Effective, and Stable Catalysts for Electrochemical Water Splitting. *Angewandte Chemie International Edition* **2015,** *54* (10), 2975-2979; (b) Jung, S.; McCrory, C. C. L.; Ferrer, I. M.; Peters, J. C.; Jaramillo, T. F., Benchmarking nanoparticulate metal oxide electrocatalysts for the alkaline water oxidation reaction. *Journal of Materials Chemistry A* **2016,** *4* (8), 3068-3076; (c) Reier, T.; Pawolek, Z.; Cherevko, S.; Bruns, M.; Jones, T.; Teschner, D.; Selve, S.; Bergmann, A.; Nong, H. N.; Schlögl, R.; Mayrhofer, K. J. J.; Strasser, P., Molecular Insight in Structure and Activity of Highly Efficient, Low-Ir Ir–Ni Oxide Catalysts for Electrochemical Water Splitting (OER). *Journal of the American Chemical Society* **2015,** *137* (40), 13031-13040.
4. Feng, L.-L.; Yu, G.; Wu, Y.; Li, G.-D.; Li, H.; Sun, Y.; Asefa, T.; Chen, W.; Zou, X., High-Index Faceted Ni3S2 Nanosheet Arrays as Highly Active and

Ultrastable Electrocatalysts for Water Splitting. *Journal of the American Chemical Society* **2015**.
5. Gerken, J. B.; Shaner, S. E.; Massé, R. C.; Porubsky, N. J.; Stahl, S. S., A survey of diverse earth abundant oxygen evolution electrocatalysts showing enhanced activity from Ni–Fe oxides containing a third metal. *Energy & Environmental Science* **2014,** *7* (7), 2376-2382.
6. Morales-Guio, C. G.; Liardet, L.; Hu, X., Oxidatively Electrodeposited Thin-Film Transition Metal (Oxy)hydroxides as Oxygen Evolution Catalysts. *Journal of the American Chemical Society* **2016,** *138* (28), 8946-8957.
7. Daojin, Z.; Xuya, X.; Zhao, C.; Nana, H.; Yin, J.; Qixian, X.; Xinxuan, D.; Tianhui, X.; Xiaolin, Z.; Xiaoming, S.; Xue, D., Flame-Engraved Nickel–Iron Layered Double Hydroxide Nanosheets for Boosting Oxygen Evolution Reactivity. *Small Methods* **2018,** *2* (7), 1800083.
8. Zhu, K.; Liu, H.; Li, M.; Li, X.; Wang, J.; Zhu, X.; Yang, W., Atomic-scale topochemical preparation of crystalline Fe3+-doped β-Ni(OH)2 for an ultrahigh-rate oxygen evolution reaction. *Journal of Materials Chemistry A* **2017,** *5* (17), 7753-7758.
9. McCrory, C. C. L.; Jung, S.; Ferrer, I. M.; Chatman, S. M.; Peters, J. C.; Jaramillo, T. F., Benchmarking Hydrogen Evolving Reaction and Oxygen Evolving Reaction Electrocatalysts for Solar Water Splitting Devices. *Journal of the American Chemical Society* **2015,** *137* (13), 4347-4357.
10. Zou, X.; Sun, Q.; Zhang, Y.; Li, G.-D.; Liu, Y.; Wu, Y.; Yang, L.; Zou, X., Ultrafast surface modification of Ni3S2 nanosheet arrays with Ni-Mn bimetallic hydroxides for high-performance supercapacitors. *Scientific Reports* **2018,** *8* (1), 4478.
11. (a) Petersen, M. A.; van den Berg, J.-A.; Ciobîcă, I. M.; van Helden, P., Revisiting CO Activation on Co Catalysts: Impact of Step and Kink Sites from DFT. *ACS Catalysis* **2017,** *7* (3), 1984-1992; (b) Fan, X.; Liu, Y.; Chen, S.; Shi, J.; Wang, J.; Fan, A.; Zan, W.; Li, S.; Goddard, W. A.; Zhang, X.-M., Defect-enriched iron fluoride-oxide nanoporous thin films bifunctional catalyst for water splitting. *Nature Communications* **2018,** *9* (1), 1809.
12. Mansour, A. N.; Melendres, C. A., XAFS investigation of the structure and valency of nickel in some oxycompounds. *Physica B: Condensed Matter* **1995,** *208-209*, 583-584.
13. (a) Chen, C. L.; Dong, C. L.; Rao, S. M.; Chern, G.; Chen, M. C.; Wu, M. K.; Chang, C. L., Investigation of the valence states of Fe and Co in Fe 1− x Co x O y (0< x <1) thin films by x-ray absorption spectroscopy. *Journal of Physics: Condensed Matter* **2008,** *20* (25), 255236; (b) Lin, K.-S.; Wang, Z.-P.; Chowdhury, S.; Adhikari, A. K., Preparation and characterization of aligned iron nanorod using aqueous chemical method. *Thin Solid Films* **2009,** *517* (17), 5192-5196.
14. Li, Y.-F.; Selloni, A., Mechanism and Activity of Water Oxidation on Selected Surfaces of Pure and Fe-Doped NiOx. *ACS Catalysis* **2014,** *4* (4), 1148-1153.
15. Luo, J.; Im, J.-H.; Mayer, M. T.; Schreier, M.; Nazeeruddin, M. K.; Park, N.-G.; Tilley, S. D.; Fan, H. J.; Grätzel, M., Water photolysis at 12.3% efficiency

via perovskite photovoltaics and Earth-abundant catalysts. *Science* **2014,** *345* (6204), 1593-1596.
16. (a) García-Osorio, D. A.; Jaimes, R.; Vazquez-Arenas, J.; Lara, R. H.; Alvarez-Ramirez, J., The Kinetic Parameters of the Oxygen Evolution Reaction (OER) Calculated on Inactive Anodes via EIS Transfer Functions: •OH Formation. *Journal of The Electrochemical Society* **2017,** *164* (11), E3321-E3328; (b) Shinagawa, T.; Garcia-Esparza, A. T.; Takanabe, K., Insight on Tafel slopes from a microkinetic analysis of aqueous electrocatalysis for energy conversion. *Scientific Reports* **2015,** *5*, 13801.
17. Chen, Y.; Yu, G.; Chen, W.; Liu, Y.; Li, G.-D.; Zhu, P.; Tao, Q.; Li, Q.; Liu, J.; Shen, X.; Li, H.; Huang, X.; Wang, D.; Asefa, T.; Zou, X., Highly Active, Nonprecious Electrocatalyst Comprising Borophene Subunits for the Hydrogen Evolution Reaction. *Journal of the American Chemical Society* **2017,** *139* (36), 12370-12373.
18. (a) Gao, Y.; Li, H.; Yang, G., Amorphous Nickel Hydroxide Nanosheets with Ultrahigh Activity and Super-Long-Term Cycle Stability as Advanced Water Oxidation Catalysts. *Crystal Growth & Design* **2015,** *15* (9), 4475-4483; (b) Smith, R. D. L.; Prévot, M. S.; Fagan, R. D.; Zhang, Z.; Sedach, P. A.; Siu, M. K. J.; Trudel, S.; Berlinguette, C. P., Photochemical Route for Accessing Amorphous Metal Oxide Materials for Water Oxidation Catalysis. *Science* **2013**.
19. Lyons, M. E. G.; Floquet, S., Mechanism of oxygen reactions at porous oxide electrodes. Part 2—Oxygen evolution at RuO2, IrO2 and IrxRu1−xO2 electrodes in aqueous acid and alkaline solution. *Physical Chemistry Chemical Physics* **2011,** *13* (12), 5314-5335.
20. (a) Qi, J.; Zhang, W.; Xiang, R.; Liu, K.; Wang, H.-Y.; Chen, M.; Han, Y.; Cao, R., Porous Nickel–Iron Oxide as a Highly Efficient Electrocatalyst for Oxygen Evolution Reaction. *Advanced Science* **2015,** *2* (10), 1500199; (b) Zaffran, J.; Toroker, M. C., Designing efficient doped NiOOH catalysts for water splitting with first principles calculations. *ChemistrySelect* **2016,** *1* (5), 911-916.
21. McCrory, C. C. L.; Jung, S.; Peters, J. C.; Jaramillo, T. F., Benchmarking Heterogeneous Electrocatalysts for the Oxygen Evolution Reaction. *Journal of the American Chemical Society* **2013,** *135* (45), 16977-16987.
22. Sagu, J. S.; Mehta, D.; Wijayantha, K. G. U., Electrocatalytic activity of CoFe2O4 thin films prepared by AACVD towards the oxygen evolution reaction in alkaline media. *Electrochemistry Communications* **2018,** *87*, 1-4.
23. Weng, B.; Xu, F.; Wang, C.; Meng, W.; Grice, C. R.; Yan, Y., A layered Na1−xNiyFe1−yO2 double oxide oxygen evolution reaction electrocatalyst for highly efficient water-splitting. *Energy & Environmental Science* **2017,** *10* (1), 121-128.
24. Swierk, J. R.; Klaus, S.; Trotochaud, L.; Bell, A. T.; Tilley, T. D., Electrochemical Study of the Energetics of the Oxygen Evolution Reaction at Nickel Iron (Oxy)Hydroxide Catalysts. *The Journal of Physical Chemistry C* **2015,** *119* (33), 19022-19029.

25. Li, Z.; Shao, M.; An, H.; Wang, Z.; Xu, S.; Wei, M.; Evans, D. G.; Duan, X., Fast electrosynthesis of Fe-containing layered double hydroxide arrays toward highly efficient electrocatalytic oxidation reactions. *Chemical Science* **2015,** *6* (11), 6624-6631.
26. Lu, Z.; Xu, W.; Zhu, W.; Yang, Q.; Lei, X.; Liu, J.; Li, Y.; Sun, X.; Duan, X., Three-dimensional NiFe layered double hydroxide film for high-efficiency oxygen evolution reaction. *Chemical Communications* **2014,** *50* (49), 6479-6482.
27. Song, F.; Hu, X., Exfoliation of layered double hydroxides for enhanced oxygen evolution catalysis. *Nature Communications* **2014,** *5*, 4477.
28. Gao, X.; Long, X.; Yu, H.; Pan, X.; Yi, Z., Ni Nanoparticles Decorated NiFe Layered Double Hydroxide as Bifunctional Electrochemical Catalyst. *Journal of The Electrochemical Society* **2017,** *164* (6), H307-H310.
29. Gong, M.; Li, Y.; Wang, H.; Liang, Y.; Wu, J. Z.; Zhou, J.; Wang, J.; Regier, T.; Wei, F.; Dai, H., An Advanced Ni–Fe Layered Double Hydroxide Electrocatalyst for Water Oxidation. *Journal of the American Chemical Society* **2013,** *135* (23), 8452-8455.
30. Ma, W.; Ma, R.; Wang, C.; Liang, J.; Liu, X.; Zhou, K.; Sasaki, T., A Superlattice of Alternately Stacked Ni–Fe Hydroxide Nanosheets and Graphene for Efficient Splitting of Water. *ACS Nano* **2015,** *9* (2), 1977-1984.
31. Zhu, X.; Tang, C.; Wang, H.-F.; Zhang, Q.; Yang, C.; Wei, F., Dual-sized NiFe layered double hydroxides in situ grown on oxygen-decorated self-dispersal nanocarbon as enhanced water oxidation catalysts. *Journal of Materials Chemistry A* **2015,** *3* (48), 24540-24546.
32. Batchellor, A. S.; Boettcher, S. W., Pulse-Electrodeposited Ni–Fe (Oxy)hydroxide Oxygen Evolution Electrocatalysts with High Geometric and Intrinsic Activities at Large Mass Loadings. *ACS Catalysis* **2015,** *5* (11), 6680-6689.